Efficiency Enhancement of Ultrathin CIGS Solar Cells by Optimal Bandgap Grading. Part III: Piecewise-Homogeneous Grading

FAIZ AHMAD[1,2], PETER B. MONK[2], AND AKHLESH LAKHTAKIA[1]

[1] The Pennsylvania State University, Department of Engineering Science and Mechanics, NanoMM–Nanoengineered Metamaterials Group, University Park, PA 16802, USA
[2] University of Delaware, Department of Mathematical Sciences, 501 Ewing Hall, Newark, DE 19716, USA

Compiled March 21, 2024

In Parts I [Appl. Opt. 58, 6067 (2019)] and II [Appl. Opt. 61, 10049 (2022)], we used a coupled optoelectronic model to optimize a thin-film CIGS solar cell with a graded-bandgap photon-absorbing layer, periodically corrugated backreflector, and multilayered antireflection coatings. Bandgap grading of the CIGS photon-absorbing layer was continuous and either linear or nonlinear, in the thickness direction. Periodic corrugation and multilayered antireflection coatings were found to engender slight improvements in the efficiency. In contrast, bandgap grading of the CIGS photon-absorbing layer leads to significant enhancement of efficiency, especially when the grading is continuous and nonlinear. However, practical implementation of continuous nonlinear grading is challenging compared to piecewise-homogeneous grading. Hence, for this study, we investigated piecewise-homogeneous approximations of the optimal linear and nonlinear grading profiles, and found that an equivalent efficiency is achieved using piecewise-homogeneous grading. An efficiency of 30.15% is predicted with a 3-layered piecewise-homogeneous CIGS photon-absorbing layer. The results will help experimentalists to implement optimal designs for highly efficient CIGS thin-film solar cells.

http://dx.doi.org/10.1364/ao.XX.XXXXXX

1. INTRODUCTION

In the two predecessor papers [1, 2], hereafter referred to as Parts I and II, a coupled optoelectronic model was used to optimize thin-film photovoltaic solar cells (PVSCs) employing $CuIn_{1-\xi}Ga_{\xi}Se_2$ (CIGS), a quaternary I-III-VI semiconductor, for the photon-absorbing layer. Three different compositional grading profiles were chosen for this layer by making ξ vary continuously with the coordinate z along the thickness direction, leading to three different types of continuous bandgap grading: (i) homogeneous, (ii) linearly graded, and (iii) nonlinearly graded. Additionally, we optimized the refractive indices and thicknesses of both a single-layered antireflection coating (SLARC) and a double-layered antireflection coating (DLARCs) for these solar cells. The projected relative enhancement, compared to the efficiency η achieved with an optimal DLARC, is modest, not exceeding 2% compared with an optimal SLARC. This suggests that a simpler SLARC may be economically preferable. In contrast, it was predicted that bandgap grading of the CIGS photon-absorbing layer can significantly enhance η, with nonlinear grading being more effective than linear grading [1, 2].

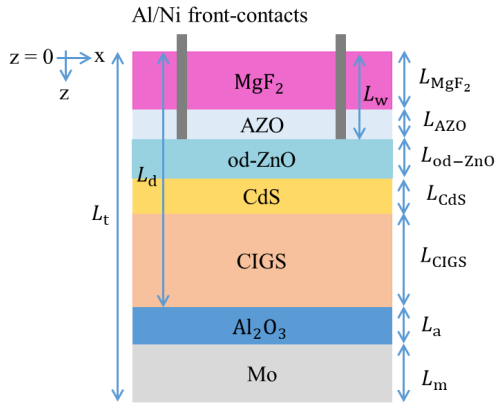

Fig. 1. Schematic of a CIGS solar cell.

The CIGS solar cell is schematically depicted in Fig. 1. Sunlight is taken to illuminate the planar face $z = 0$ of the magnesium-fluoride layer of thickness $L_{MgF_2} = 110$ nm serving

as the SLARC. Then come in succession an aluminum-doped zinc-oxide layer of thickness $L_{\text{AZO}} = 100$ nm, an oxygen-deficient zinc-oxide layer of thickness $L_{\text{od-ZnO}} = 80$ nm, a cadmium-sulfide layer of thickness $L_{\text{CdS}} = 70$ nm, a CIGS layer of thickness L_{CIGS}, an aluminum-oxide layer of thickness $L_{\text{a}} = 50$ nm, and a molybdenum layer of thickness $L_{\text{m}} = 500$ nm. The best efficiency had been obtained in Part II with $L_{\text{CIGS}} = 2200$ nm, which value was also chosen here. Thus, the total thickness of the multilayered structure is $L_{\text{t}} = 3110$ nm.

If the bandgap energy is linearly graded in the CIGS layer, it can be expressed as [2]

$$\begin{aligned} \mathsf{E}_{\text{g}}(z) &= \mathsf{E}_{\text{g,min}} \\ &+ A\left(\mathsf{E}_{\text{g,max}} - \mathsf{E}_{\text{g,min}}\right) \frac{z - (L_{\text{w}} + L_{\text{od-ZnO}} + L_{\text{CdS}})}{L_{\text{CIGS}}}, \\ & z \in [L_{\text{w}} + L_{\text{od-ZnO}} + L_{\text{CdS}}, L_{\text{d}}], \end{aligned} \tag{1}$$

where $\mathsf{E}_{\text{g,min}}$ is the minimum bandgap energy, $\mathsf{E}_{\text{g,max}} = 1.626$ eV is the maximum bandgap energy, A is an amplitude (with $A = 0$ representing a homogeneous CIGS layer), $L_{\text{w}} = L_{\text{MgF}_2} + L_{\text{AZO}}$, and $L_{\text{d}} = L_{\text{w}} + L_{\text{od-ZnO}} + L_{\text{CdS}} + L_{\text{CIGS}}$. The nonlinear grading is modeled as [2]

$$\begin{aligned} &\mathsf{E}_{\text{g}}(z) = \mathsf{E}_{\text{g,min}} + A\left(\mathsf{E}_{\text{g,max}} - \mathsf{E}_{\text{g,min}}\right) \\ &\times \left\{\frac{1}{2}\left[\sin\left(2\pi K \frac{z - (L_{\text{w}} + L_{\text{od-ZnO}} + L_{\text{CdS}})}{L_{\text{CIGS}}} - 2\pi\psi\right) + 1\right]\right\}^{\alpha}, \\ &\qquad z \in [L_{\text{w}} + L_{\text{od-ZnO}} + L_{\text{CdS}}, L_{\text{d}}], \end{aligned} \tag{2}$$

where $\psi \in [0,1]$, $K > 0$, and $\alpha > 0$. Figures 2(a) and (b), respectively, show

- the optimal linear grading profile, with $\mathsf{E}_{\text{g,min}} = 0.96$ eV and $A = 1$ in Eq. (1) giving $\eta = 24.17\%$, and
- the optimal nonlinear grading profile, with $\mathsf{E}_{\text{g,min}} = 1.07$ eV, $A = 1$, $\alpha = 8$, $K = 0.6$, and $\psi = 0.36$ in Eq. (2) giving $\eta = 29.98\%$.

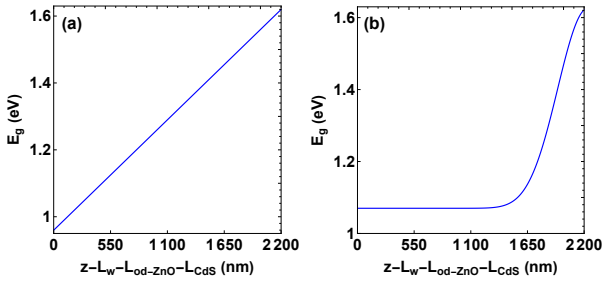

Fig. 2. Optimal (a) linear and (b) nonlinear bandgap-energy profiles in the CIGS photon-absorbing layer [2].

The continuous variation of E_{g} with z in the CIGS photon-absorbing layer helps in capturing a wider solar spectrum [3] and creating an additional drift field for better collection of charge carriers [4]. However, a continuously varying $\mathsf{E}_{\text{g}}(z)$ will create manufacturing complexity [5] leading to additional cost. A way must be found to achieve the benefits of bandgap grading without increasing the manufacturing complexity and cost. In this study, therefore we explored the implementation of bandgap grading in the CIGS photon-absorbing layer using the following three piecewise-homogeneous approaches, in each of which that layer was divided into $n_{\text{sub}} \geq 1$ homogeneous sublayers.

- Approach 1: *Piecewise-homogeneous approximation of optimal linear grading profile.* The optimal linear grading profile in Fig. 2(a) was replaced by one comprising n_{sub} homogeneous sublayers of equal thickness $L_{\text{CIGS}}/n_{\text{sub}}$. The bandgap energy E_{g_j} in the j$^{\text{th}}$ sublayer, $j \in \{1, 2, \cdots, n_{\text{sub}}\}$, was set equal to the value of $\mathsf{E}_{\text{g}}(z)$ calculated using Eq. (1) at the midpoint of that specific sublayer, as illustrated in Fig. 3 for $n_{\text{sub}} \in \{3, 5, 7, 9\}$.

- Approach 2: *Piecewise-homogeneous approximation of optimal nonlinear grading profile.* The optimal nonlinear grading profile in Fig. 2(b) required a different treatment. The CIGS layer was partitioned into $n_{\text{sub}} = m_{\text{sub}} + 1$ homogeneous sublayers. The first sublayer was chosen to be 1500-nm thick with uniform bandgap energy $\mathsf{E}_{\text{g}_1} = 1.07$ eV, in consonance with Fig. 2(b). The remainder $z - L_{\text{w}} - L_{\text{od-ZnO}} - L_{\text{CdS}} \in (1500, 2200)$ nm was divided into $m_{\text{sub}} \geq 2$ homogeneous sublayers of equal thickness, with bandgap energy E_{g_j} in the j$^{\text{th}}$ sublayer, $j \in \{2, 3, \cdots, n_{\text{sub}}\}$, set equal to the value of $\mathsf{E}_{\text{g}}(z)$ calculated using Eq. (2) at the midpoint of that specific sublayer, as illustrated in Fig. 4 for $m_{\text{sub}} \in \{2, 4, 6, 8\}$.

- Approach 3: *Optimal piecewise-homogeneous grading profile.* Lastly, the CIGS photon-absorbing layer was divided into n_{sub} sublayers, the j$^{\text{th}}$ sublayer, $j \in \{1, 2, \cdots, n_{\text{sub}}\}$, of thickness $L_j \in [0, 2200]$ nm, each with uniform bandgap energy $\mathsf{E}_{\text{g}_j} \in [0.947, 1.626]$ eV, subject to the constraint

$$\sum_{j=1}^{n_{\text{sub}}} L_j = L_{\text{CIGS}}. \tag{3}$$

The $2n_{\text{sub}}$ quantities $\left\{\mathsf{E}_{\text{g}_j}, L_j\right\}_{j=1}^{n_{\text{sub}}}$ were determined by the differential evolution algorithm [7, 8] for maximizing η.

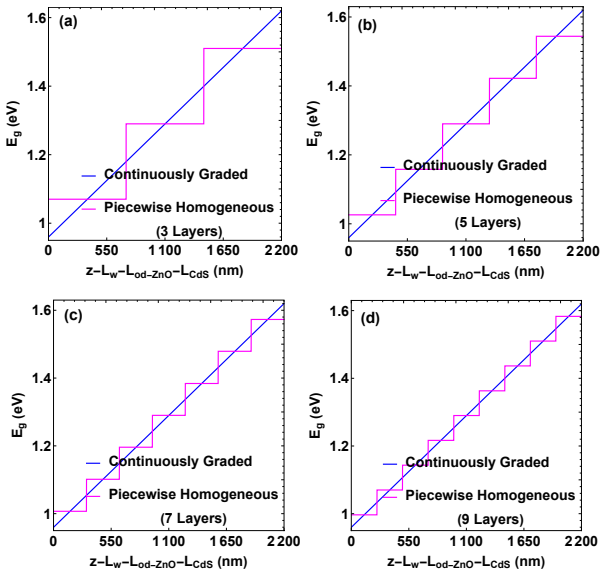

Fig. 3. Piecewise-homogeneous approximations (pink lines) of the optimal linear grading profile (blue lines) given by Eq. (1) in the CIGS photon-absorbing layer for (a) $n_{\text{sub}} = 3$, (b) $n_{\text{sub}} = 5$, (c) $n_{\text{sub}} = 7$, and (d) $n_{\text{sub}} = 9$.

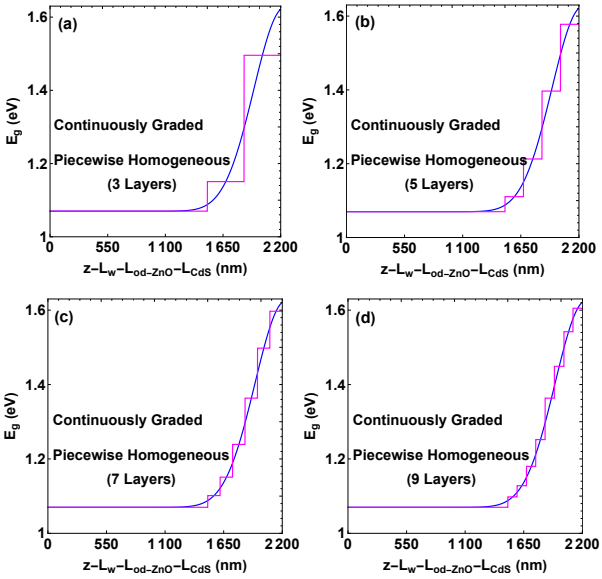

Fig. 4. Piecewise-homogeneous approximations (pink lines) of the optimal nonlinear grading profile (blue lines) given by Eq. (2) in the CIGS photon-absorbing layer for (a) $n_{\text{sub}} = 3$, (b) $n_{\text{sub}} = 5$, (c) $n_{\text{sub}} = 7$, and (d) $n_{\text{sub}} = 9$.

This paper is organized as follows. The optoelectronic modeling of the solar cell is briefly mentioned in Sec. 2. Numerical results are presented and discussed in Sec. 3, divided into three subsections. Section 3.A is devoted to Approach 1, Sec. 3 B to Approach 2, and Section 3.C to Approach 3 for piecewise-homogeneous CIGS photon-absorbing layer. The paper ends with concluding remarks in Sec. 4.

2. OPTOELECTRONIC MODEL

The CIGS solar cell has a MgF_2/AZO/od-ZnO/CdS/CIGS/Al_2O_3/Mo multilayered structure shown in Fig. 1 [1, 2]. The optical description remains unchanged from Part II. Complete details of optical calculations and the spectrums of the real and imaginary parts of the relative permittivity $\varepsilon(\lambda_0)/\varepsilon_0$ of all the materials used in our calculations are available in Part I [1] and Ref. 6. The electrical description and calculations remain unchanged from Part II [2].

3. NUMERICAL RESULTS AND DISCUSSION

A. Approach 1: Piecewise-homogeneous approximation of optimal linear grading profile.

First, we considered the most efficient CIGS solar cell in which the CIGS layer has linearly graded bandgap energy given by Eq. (1), as detailed in Part II [2]. The optimal parameters for this design resulted in efficiency $\eta = 24.17\%$, with corresponding values of short-circuit current density $J_{\text{sc}} = 36.38$ mA cm^{-2}, open-circuit voltage $V_{\text{oc}} = 810$ mV, and fill factor FF = 82% [2], as outlined in Table 1.

We implemented piecewise-homogeneous approximations of the optimal linear grading profile with $n_{\text{sub}} \geq 1$. Computed values of η, J_{sc}, V_{oc}, and FF for $n_{\text{sub}} \in \{1, 3, 5, 7, 9\}$ are presented in Table 2. The table also includes values of $\mathsf{E}_{g_j} = \mathsf{E}_g(z_j)$ and $L_j = L_{\text{CIGS}}/n_{\text{sub}}$, $j \in \{1, 2, \cdots, n_{\text{sub}}\}$, for the n_{sub} sublayers, with z_j denoting the midpoint of the j$^{\text{th}}$ sublayer. No additional optimization was done.

For $n_{\text{sub}} = 1$, $\mathsf{E}_{g_1} = 1.29$ eV and $L_1 = L_{\text{CIGS}}$. The predicted efficiency for this design is 17.46%, with $J_{\text{sc}} = 27.87$ mA cm^{-2}, $V_{\text{oc}} = 770$ mV, and FF = 81%. For $n_{\text{sub}} = 3$, η rises to 24.07%, exhibiting a relative enhancement of 37.85% compared to a single homogeneous CIGS layer ($n_{\text{sub}} = 1$). Concurrently, J_{sc} increases from 27.87 mA cm^{-2} to 35.87 mA cm^{-2} (a 28.70% relative increase), V_{oc} from 770 mV to 790 mV (a 2.59% relative increase), and FF from 81 to 85 (a 4.94% relative increase). The predicted efficiency is only slightly lower than for the continuous linearly graded bandgap CIGS photon-absorbing layer ($\eta = 24.17\%$) in Table 1. Similarly, for $n_{\text{sub}} = 5$, $n_{\text{sub}} = 7$, and $n_{\text{sub}} = 9$ in Table 2, efficiencies of 24.32%, 23.49% and 24.63%, respectively, were obtained, showing relative enhancements of 39.29%, 34.54% and 41.06% compared to the single homogeneous CIGS layer ($n_{\text{sub}} = 1$).

These data suggest that optimal linear grading profile can be approximated very well by a piecewise-homogeneous grading profile with $n_{\text{sub}} \geq 3$. The design procedure could very simply be.as follows: Use the optoelectronic model with Eq. (1) for the CIGS photon-absorbing layer; determine $\mathsf{E}_{\text{g,min}}$ and A to maximize η; and adopt Approach 1 with n_{sub} as small as three for piecewise-homogeneous approximation for industrial implementation. That approximation is not going to substantially lower the efficiency.

Table 1. Predicted parameters of the optimal CIGS solar cell when the 2200-nm-thick CIGS photon-absorbing layer is either linearly graded [Eqs. (1)] or nonlinearly graded [Eq. (2)].

Grading type	$\mathsf{E}_{\text{g,min}}$ (eV)	A	α	K	ψ	J_{sc} (mA cm^{-2})	V_{oc} (mV)	FF (%)	η (%)
Linear	0.95	0.98	-	-	-	36.38	810	82	24.17
Nonlinear	1.07	1.0	8	0.60	0.36	38.02	980	80	29.98

Table 2. Bandgap energies and thicknesses of sublayers along with predicted performance parameters when Approach 1 is implemented.

n_{sub}	E_{g_1} / L_1 (eV)/ (nm)	E_{g_2} / L_2 (eV)/ (nm)	E_{g_3} / L_3 (eV)/ (nm)	E_{g_4} / L_4 (eV)/ (nm)	E_{g_5} / L_5 (eV)/ (nm)	E_{g_6} / L_6 (eV)/ (nm)	E_{g_7} / L_7 (eV)/ (nm)	E_{g_8} / L_8 (eV)/ (nm)	E_{g_9} / L_9 (eV)/ (nm)	J_{sc} (mA cm^{-2})	V_{oc} (mV)	FF (%)	η (%)	Relative change in η (%)
1	1.29/ 2200	-	-	-	-	-	-	-	-	27.87	770	81	17.46	
3	1.07/ 733.33	1.29/ 733.33	1.51/ 733.33	-	-	-	-	-	-	35.87	790	85	24.07	37.85
5	1.026/ 440	1.158/ 440	1.29/ 440	1.422/ 440	1.544/ 440	-	-	-	-	36.19	810	83	24.32	39.29
7	1.007/ 314.28	1.1014/ 314.28	1.196/ 314.28	1.29/ 314.28	1.384/ 314.28	1.479/ 314.28	1.5729/ 314.28	-	-	36.26	810	80	23.49	34.54
9	0.9966/ 244.44	1.07/ 244.44	1.1433/ 244.44	1.2166/ 244.44	1.29/ 244.44	1.363/ 244.44	1.4366/ 244.44	1.51/ 244.44	1.583/ 244.44	36.32	820	83	24.63	41.06

B. Approach 2: Piecewise-homogeneous approximation of optimal nonlinear grading profile.

Next, we considered the most efficient CIGS solar cell in which the CIGS layer has nonlinearly graded bandgap energy given by Eq. (2), as detailed in Part II [2]. The optimal parameters for this design resulted in $\eta = 29.98\%$, with corresponding values of $J_{sc} = 38.02$ mA cm^{-2}, $V_{oc} = 980$ mV, and FF $= 80\%$ [2], as outlined in Table 1.

We then implemented piecewise-homogeneous approximations of the optimal nonlinear grading profile with $n_{sub} \geq 1$. No additional optimization was done. Computed values of η, J_{sc}, V_{oc}, and FF for $n_{sub} \in \{1, 3, 5, 7, 9\}$ are presented in Table 3. The table also includes values of E_{g_j} and L_j, $j \in \{1, 2, \cdots, n_{sub}\}$, for the n_{sub} sublayers.

For $n_{sub} = 1$, the mean of the nonlinearly graded bandgap profile is $E_g = 1.15$ eV, serving as a reference for higher values of n_{sub}. The predicted efficiency for this design is 18.02%, with $J_{sc} = 32.99$ mA cm^{-2}, $V_{oc} = 660$ mV, and FF $= 83\%$, as noted in Table 3. For $n_{sub} = 3$, an efficiency of 28.11% was predicted, demonstrating a substantial relative enhancement of 55.99% compared to a single homogeneous CIGS layer with bandgap energy that is the mean of nonlinearly graded bandgap energy ($n_{sub} = 1$). Simultaneously, J_{sc} increases from 32.99 mA cm^{-2} to 38.03 mA cm^{-2} (a 15.28% relative increase), V_{oc} from 660 mV to 930 mV (a 40.91% relative increase), and FF from 81% to 79.5% (a 1.85% relative decrease). The efficiency predicted with $n_{sub} = 3$ is 6.24% lower than for the continuous nonlinearly graded bandgap CIGS photon-absorbing layer ($\eta = 29.98\%$) in Table 1.

Table 3. Bandgap energies and thicknesses of sublayers along with predicted performance parameters when Approach 2 is implemented.

n_{sub}	E_{g_1} / L_1 (eV)/ (nm)	E_{g_2} / L_2 (eV)/ (nm)	E_{g_3} / L_3 (eV)/ (nm)	E_{g_4} / L_4 (eV)/ (nm)	E_{g_5} / L_5 (eV)/ (nm)	E_{g_6} / L_6 (eV)/ (nm)	E_{g_7} / L_7 (eV)/ (nm)	E_{g_8} / L_8 (eV)/ (nm)	E_{g_9} / L_9 (eV)/ (nm)	J_{sc} (mA cm^{-2})	V_{oc} (mV)	FF (%)	η (%)	Relative change in η (%)
1	1.15/ 2200	-	-	-	-	-	-	-	-	32.99	660	83	18.02	
3	1.07/ 1500	1.151/ 350	1.496/ 350	-	-	-	-	-	-	38.03	930	79.5	28.11	55.99
5	1.07/ 1500	1.111/ 175	1.213/ 175	1.397/ 175	1.577/ 175	-	-	-	-	38.04	880	75	25.23	40.01
7	1.07/ 1500	1.101/ 116.66	1.151/ 116.66	1.239/ 116.66	1.363/ 116.66	1.498/ 116.66	1.597/ 116.66	-	-	38.03	870	78	25.70	42.62
9	1.07/ 1500	1.098/ 87.5	1.128/ 87.5	1.18/ 87.5	1.252/ 87.5	1.3634/ 87.5	1.449/ 87.5	1.5425/ 87.5	1.605/ 87.5	38.03	880	78	26.07	44.67

Similarly, for $n_{sub} = 5$, $n_{sub} = 7$, and $n_{sub} = 9$ in Table 3, efficiencies of 25.23%, 25.70%, and 26.07%, respectively, were obtained, showing relative enhancements of 40.01%, 42.62%, and 44.67% compared to the efficiency predicted for $n_{sub} = 1$. However, about $15 \pm 1\%$ lower efficiencies than the continuous nonlinearly graded bandgap CIGS photon-absorbing layer ($\eta = 29.98\%$) in Table 1 are predicted with Approach 2.

Overall, the introduction of a nonlinearly graded CIGS layer approximated with several piecewise homogeneous sublayers is predicted to exhibit significant improvement compared to a single homogeneous CIGS absorber layer with $n_{sub} = 1$. Despite that, the predicted efficiencies fall between 6.24% and 15.78% lower than for the continuous nonlinearly graded CIGS layer ($\eta = 29.98\%$ in Table 1). However, it is worth noting that a 28% efficiency can be attained with only a 3-layered piecewise homogeneous CIGS photon-absorbing layer, indicating the potential for reduced fabrication complexity with a relative compromise of only 6% in device performance compared to a continuous nonlinearly graded CIGS layer.

Parenthetically, η in Table 2 does not monotonically increase to 24.17% in Table 1 as n_{sub} increases. Likewise, η in Table 3 does not monotonically increase to 29.98% in Table 1 as n_{sub} increases. Numerical experiments with the optoelectronic model indicate that the absence of a monotonic increase is largely due to the nonlinearity introduced in the equations for charge-carrier transport by the recombination of electrons and holes [9].

C. Approach 3: Optimal piecewise-homogeneous grading profile.

Lastly, the third approach is completely different from the first and the second approaches, in that an optimal continuous grading profile, whether linear or nonlinear, was not approximated. Instead, the CIGS layer was divided into n_{sub} sublayers, each of unknown thickness and uniform bandgap energy. The quantities $\left\{E_{g_j}, L_j\right\}_{j=1}^{n_{sub}}$ were determined by optimizing η. Thus, Approach 3 calls for *de-novo* optimization instead of approximating an optimal continuous grading profile.

The optimal design identified with $n_{sub} = 3$ requires $E_{g_1} = 1.12$ eV, $E_{g_2} = 1.151$ eV, $E_{g_3} = 1.6$ eV, $L_1 = 1500$ nm, $L_2 = 350$ nm, and $L_3 = 350$ nm. This design promises an efficiency of 30.15%, showing a remarkable relative enhancement greater than 55% compared to a single homogeneous CIGS absorber layer with $n_{sub} = 1$ in Tables 1 and 2. Both J_{sc} and V_{oc} improve, the latter more remarkably. The predicted efficiency of 30.15% is even greater than for the continuous nonlinearly graded CIGS layer ($\eta = 29.98\%$) in Table 1. This 0.57% relative improvement in efficiency is a result of the optimal selection of thicknesses and bandgap energies of the sublayers of the CIGS photon-absorbing layer in Approach 3, contrasting with the use of fixed values of those parameters in Approach 2.

The spatial profile of $E_g(z)$ for $n_{sub} = 3$ is presented in Fig. 5. Notably, this profile is similar, but not the same as, the optimal nonlinearly graded profile predicted in Part II and shown in Fig. 4.

The use of $n_{sub} > 3$ did not return higher η in Approach 3, this feature also being shared by Approach 2. Approach 1 does promise the highest value of η with $n_{sub} = 9$ in Table 2, but that approach deliver significantly lower efficiencies than Approaches 2 and 3. Additionally, it is worth highlighting that a piecewise homogeneous CIGS photon-absorbing layer with only three sublayers offers a reduction in fabrication complexity without compromising device performance.

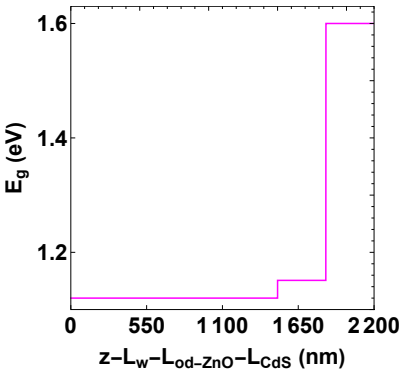

Fig. 5. Optimal piecewise-homogeneous grading profile for the CIGS photon-absorbing layer delivered by Approach 3 for $n_{\text{sub}} = 3$.

4. CONCLUDING REMARKS

In Parts I and II, we used a coupled optoelectronic model to optimize a thin-film CIGS solar cell with a graded-bandgap photon-absorbing layer, periodically corrugated backreflector, and multilayer antireflection coatings. Bandgap grading of the CIGS photon-absorbing layer was either continuous linear or continuous nonlinear in the thickness direction. For the present study, we implemented piecewise-homogeneous approximations of the bandgap-grading profiles of the optimal CIGS layers from Parts I and II, and we found that the approximations can deliver just about as much efficiency as their unapproximated counterparts. The *de-novo* optimization in Approach 3 instead of approximating an optimal continuous grading profile in Approaches 1 and 2 delivered the highest efficiency. The simplicity of piecewise homogeneity compared to continuous variation facilitates practical implementation, providing valuable insights for experimentalists aiming to realize highly efficient CIGS thin-film solar cells, including bifacial ones [10].

Acknowledgments. A. Lakhtakia thanks the Charles Godfrey Binder Endowment at the Pennsylvania State University for ongoing support of his research. The research of A. Lakhtakia was partially supported by US National Science Foundation (NSF) under grant number DMS-2011996. The research of F. Ahmad and P. B. Monk was supported by the US NSF under grant number DMS-2011603.

Funding. US National Science Foundation (DMS-2011996 and DMS-2011603)

Disclosures. The authors declare no conflicts of interest.

REFERENCES

1. F. Ahmad, T. H. Anderson, P. B. Monk, and A. Lakhtakia, "Efficiency enhancement of ultrathin CIGS solar cells by optimal bandgap grading," Appl. Opt. **58**, 6067–6078 (2019).
2. F. Ahmad, A. Lakhtakia, B. J. Civilletti, and P. B. Monk, "Efficiency enhancement of ultrathin CIGS solar cells by optimal bandgap grading. Part II: finite-difference algorithm and double-layer antireflection coatings," Appl. Opt. **61**, 10049–10061 (2022).
3. I. M. Dharmadasa, "Third generation multi-layer tandem solar cells for achieving high conversion efficiencies," Sol. Energy Mater. Sol. Cells **85**, 293–300 (2005).
4. O. Lundberg, M. Edoff, and L. Stolt, "The effect of Ga-grading in CIGS thin film solar cells," Thin Solid Films **480–481**, 520–525 (2005).
5. I. L. Repins, S. Harvey, K. Bowers, S. Glynn, and L. M. Mansfield, "Predicting Ga and Cu profiles in co-evaporated Cu(In,Ga)Se_2 using modified diffusion equations and a spreadsheet," MRS Adv. **2**, 3169–3174 (2017).
6. F. Ahmad, A. Lakhtakia, and P. B. Monk, *Theory of Graded-Bandgap Thin-Film Solar Cells* (Morgan & Claypool, 2021).
7. R. Storn and K. Price, "Differential evolution—a simple and efficient heuristic for global optimization over continuous spaces," J. Global Optim. **11**, 341–359 (1997).
8. Bilal, M. Pant, H. Zaheer, L. Garcia-Hernandez, and A. Abraham, "Differential evolution: A review of more than two decades of research," Engg. Appl. Artif. Intell. **90**, 103479 (2020).
9. F. Ahmad, B. J. Civiletti, P. B. Monk, and A. Lakhtakia, "Effects of defect density, minority carrier lifetime, doping density, and absorber-layer thickness in CIGS and CZTSSe thin-film solar cells," J. Photon. Energy **13**, 025502 (2023).
10. F. Ahmad, P. B. Monk, and A. Lakhtakia, "Bifacial flexible CIGS thin-film solar cells with nonlinearly graded-bandgap photon-absorbing layers," J. Phys. Energy **6**, 025012 (2024).